INSTITUTE OF PHYSICS PUBLISHING NETWORK: COMPUTATION IN NEURAL SYSTEMS

Network: Comput. Neural Syst. **13** (2002) 283–310 PII: S0954-898X(02)37528-6

A shape analysis framework for neuromorphometry

Luciano da Fontoura Costa[1], **Edson Tadeu Monteiro Manoel**[1], **Fabien Faucereau**[2], **Jamel Chelly**[2], **Jaap van Pelt**[3] **and Ger Ramakers**[3]

[1] Cybernetic Vision Research Group, Instituto de Física de São Carlos, University of São Paulo, Caixa Postal 369, São Carlos, SP, 13560-970, Brazil
[2] INSERM Unite 129—ICGM, CHU Cochin, Paris, France
[3] Neurons and Networks, Netherlands Institute of Brain Research, Meibergdreef 33, 1105 AZ Amsterdam, The Netherlands

Received 21 December 2001
Published 15 July 2002
Online at stacks.iop.org/Network/13/283

Abstract

This paper addresses in an integrated and systematic fashion the relatively overlooked but increasingly important issue of measuring and characterizing the geometrical properties of nerve cells and structures, an area often called neuromorphology. After discussing the main motivation for such an endeavour, a comprehensive mathematical framework for characterizing neural shapes, capable of expressing variations over time, is presented and used to underline the main issues in neuromorphology. Three particularly powerful and versatile families of neuromorphological approaches, including differential measures, symmetry axes/skeletons, and complexity, are presented and their respective potentials for applications in neuroscience are identified. Examples of applications of such measures are provided based on experimental investigations related to automated dendrogram extraction, mental retardation characterization, and axon growth analysis.

'*... the functional superiority of the human brain is intimately linked up with the prodigious abundance and unaccustomed wealth of forms of the so-called neurons with short axons.*' (*Recollections of My Life*, Santiago Ramon y Cajal)

1. Introduction

- How can 3D representations of nerve cells be obtained automatically?
- How many classes of nerve cells are there in the human brain?
- How does neural shape change along the lifetime of an animal?
- How can morphologically realistic neural models be obtained?
- How do neural shape and function relate to one another?

Although these are scientifically relevant questions, no answers can be found in the literature. This situation is all the more surprising given the unprecedented scientific and technological advances accomplished in neuroscience during the last century, indicating that the problem of neural shape, at least from a quantitative perspective, has been overlooked during that same period. After a head start with the pioneering works of Cajal [1], the issue of neural shape was overshadowed by the impressive success of the electrophysiological techniques introduced soon afterwards. However, even if electrophysiological processes may in the end account for most of brain behaviour, the study of neural shape is still important for several reasons including diagnosis, investigation of mechanisms underlying learning and memory, and analysis of neural regeneration. Moreover, a growing body of evidence has clearly indicated that neural shape and function exhibit a strong interrelationship [2–9], motivating a series of further investigations involving shape characterization. Yet, in addition to the remarkable success of electrophysiology, the lack of automated computational morphological methods has severely restricted neural shape investigation, to the extent that experimental investigations often involve manual reconstructions and measures.

As we step into the 21st century, and now duly backed by a considerable knowledge of the electrophysiological properties of the nervous system as well as the maturity of shape analysis approaches, the time is ripe to resume attention to Cajal's initial interest in the relationship between neural shape and behaviour. Indeed, the steadily growing number of related publications (e.g. [2–9]), as well as the *Quantitative Neuroanatomy Tools Workshop* recently hosted by the Netherlands Institute for Brain Research, indicate that this process has indeed started already. The present article addresses the important issue of neural shape measurement and analysis from an integrated and more sophisticated perspective. Here we demonstrate that by using powerful and sound measures in combination with automatic shape analysis procedures it is possible to achieve a more comprehensive and detailed quantitative analysis of neuronal shapes than with current manual reconstruction techniques and shape descriptors, bringing quantitative neuromorphology to a higher level of sophistication. However, before proceeding further with this issue, it is important to review some of the main reasons that neural shape should receive attention.

Classification and diagnosis. Even if neural shape and function were completely independent of one another, the morphology of the neurons in the nervous system would still be relevant as a resource for anatomical investigation and organization, especially regarding the identification of neural tissues and domains. For instance, the cytoarchitecture of the neocortex is strongly defined by the morphological classes of neurons found along the cortical stratification. In addition, the accurate morphological characterization of nerve cells can provide valuable information for delineating morphological classes to be correlated with functional classes, as well as for the diagnosis of several neurological pathologies. It is therefore important to have suitable measures capable of expressing the relevant specific geometrical features in such a way as to properly discriminate among the cell classes.

Neural development. Nerve cells reflect a highly intricate dynamic evolution, which is governed by *intrinsic* and *extrinsic* factors. Respective examples of these include the genetic content and fields/waves (e.g. electric fields, ionic waves, and even gravity). In addition, growing cells impose geometrical and physical constraints on one another. It is the interaction of such influences through time and space that determines the evolution of neural shape, including synaptogenesis. As a consequence, the proper understanding of these important processes requires the use of morphological measures and tools applied over sequences of images of developing nerve cells and structures.

Shape/function relationship. An increasing body of evidence has supported a close relationship between the morphological and functional properties of neurons, including the well-known example of the correspondence between the morphological and functional classes of cat retinal ganglion cells [3, 10–14]. While the geometry of neurons could be no more than a by-product of the cell type and history of received stimuli processed through the synapses, there is growing evidence for *volume transmission* [15, 16], which considers electrochemical interactions occurring along the whole cell membrane, not restricted to the synaptic contacts.

Neuromorphic modelling. In order to investigate the above possibilities, it is important to develop computational models of the nervous system that take into account the intricacies of neural geometry. Present computational studies [17–19] underscore the importance of neuronal shape in the processing and integration of postsynaptic potentials, which requires better knowledge of neuronal shape details. Because of their active membrane properties, signal integration in dendritic trees is highly complex, making the issue and the role of morphology under continuously changing dynamic states of the membrane a non-trivial endeavour. The main advantage of obtaining geometrically precise models of neural structures is that we not only know everything about their characteristics and connections, but also can change these at will in order to investigate how neuronal function is affected by morphological changes. Both static and dynamic models, the latter characterized by neural shape that changes with time, can be obtained, paving the way for a myriad of possible investigations.

In spite of all these demands and promising perspectives, much remains to be done in neuromorphological research. To begin with, there is no agreement on an established set of measures to be used in specific types of investigation. Indeed, most of the existing measures are somewhat empirical and are frequently extracted manually. As a consequence, the fundamental questions posed at the beginning of this article have not been properly answered yet. It is felt that it is now time to apply the technological advances in neuroscience and computer vision achieved during the last few decades in an integrated and systematic reconsideration of Cajal's original motivation. The current work addresses the above motivation and demands, concentrating on the issue of automated neuromorphology, i.e. the use of geometrical measures to characterize properties of nerve cells and structures. While partially relying on recently introduced concepts and techniques, and consequently representing a review of the authors own related work, the current work also incorporates a series of novel contributions, including the use of multiscale spectral differential geometry techniques for accurate characterization of the arc length and speed of growing processes and the characterization of geometrical complexity of arborizations of neural structures in terms of the multiscale fractal dimension, which has been applied as a powerful means for analysing and categorizing the morphology of nerve cells in retardation.

The paper starts by presenting a sound and comprehensive mathematical framework, based on dynamic systems concepts, that can be used to underlie the several neuromorphological issues considered in this work. Then, after briefly characterizing the acquisition and pre-processing of neural images, the three families of neuromorphological measures are presented and discussed. These include: differential geometry measures, based on the extensive mass of knowledge derived from differential calculus; symmetry axes and skeletons, based on the discrete geometry concept of exact dilations; and objective approaches to complexity. The main potential of each of these measure families is identified with respect to promising specific applications in neuroscience.

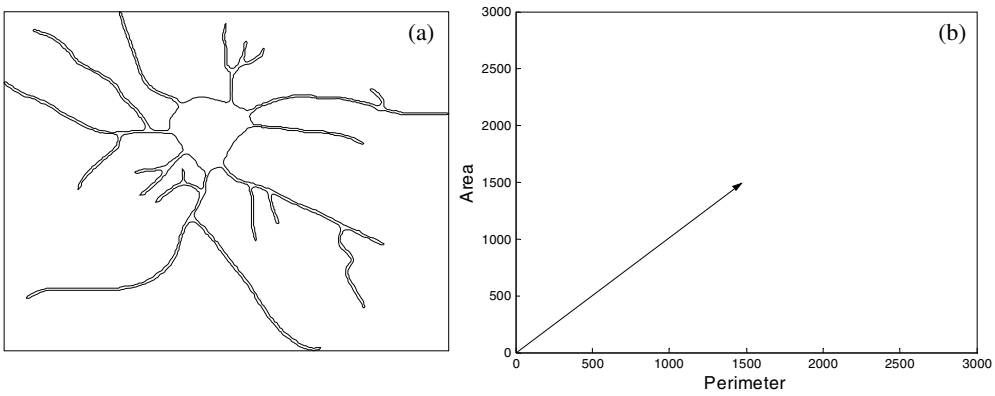

Figure 1. A nerve cell (a) and its characterization as a vector in the area/perimeter feature space (b).

2. Mathematical basis

This section presents a unifying mathematical formulation which takes into account the inherent variability of neural geometry through time and space and therefore allows the proper and effective characterization of several of the key issues in dynamic neuromorphology. Let the shape of a specific 2D neuron, illustrated in figure 1, be *characterized* by the vector (ordered set of quantities) $\vec{S} = [f_1,\ f_2, \ldots, f_N]$ where f_i stands for any measurement, ranging from very elementary ones, like absolute pixel positions, to measurements like area, perimeter, and curvature. By 'characterized' it is meant that the vector $\vec{S}$ is capable of expressing especially interesting *properties* (also called *measures* or *features*) of the shape, such as its size, complexity, and number of branches, represented by the components of the vector. In the case where $\vec{S}$ incorporates a set of measures capable of allowing the original shape to be reconstructed to a certain high degree of accuracy, defined for each specific case, $\vec{S}$ can be said to provide a *complete representation* of the original shape. There are several possible such representations of shapes (see, for instance, [20]), the most trivial being the set of all possible points belonging to the shape. Although such a representation implies an infinite number of points for shapes in continuous spaces, spatially sampled shapes are characterized in terms of a finite number of sampled points. Alternative interesting complete shape representations include the Fourier coefficients and the curvature values along the shape [20], which can also be accomplished by using a finite number of values for the case of shapes represented in digital images.

Given a neural shape, its respective characterization/representation in terms of the vector $\vec{S}$ can be nicely displayed as a vector in the respective N-dimensional feature (or phase) space. For instance, in the case where we define $\vec{S} =$ [perimeter, area], the original neuron will be characterized by a vector, as illustrated in figure 1. Now, the characterization of the *temporal evolution* of a neuron can be represented by a *trajectory* through the respective phase space, as illustrated in figure 2 with respect to a hypothetical shape unfolding obtained by Gaussian smoothing of an adult cell. More realistic situations are considered in the following sections of this paper. Likewise, neurons belonging to two distinct neural classes can be characterized by clouds of points in the phase space, as in figure 3. Provided that the measures are sound, vectors defined by similar neurons will fall close to one another in the phase space, while those corresponding to different neurons will tend to be distant from one another. In other words, the Euclidean distance in the phase space is related to the dissimilarity between the geometry

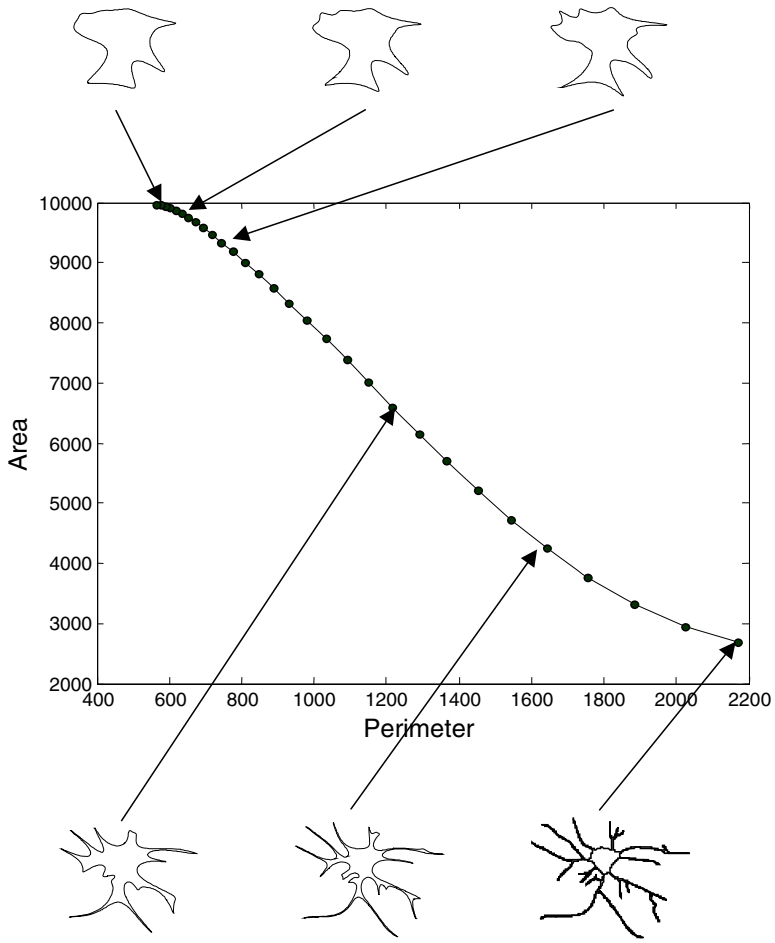

Figure 2. The geometrical changes experienced by a neural shape through time, as illustrated in this hypothetical example obtained through Gaussian smoothing of an adult cell, can be suitably represented in terms of a parametrized trajectory in a feature space (in this case area/perimeter).

of the respective cells. It is therefore natural to understand the problem of *classifying* nerve cells as the procedure of clustering the respective vectors in the phase space. For instance, the situation depicted in figure 3 can be clearly understood as involving two classes of neurons.

The above framework can be easily extended to characterize *cell differentiation*. First, it is necessary to introduce the concept of *potential space*, which corresponds to the region of the feature space covered by all the possible differentiations of a specific type of precursor cell at time t, which is illustrated as the set in the area/perimeter plane defined for $t = 0$ in figure 4. The process of cell differentiation can now be properly characterized in terms of the evolution of the respective potential spaces through time, which is explicitly indicated in a new added axis.

Finally, the concept of phase space representation in terms of vectors can be easily adapted to allow statistical characterization of the observed cells by adopting the concept of probability density functions. Let us introduce this possibility through the following example. Let a set of M neurons of a specific type have their perimeter and area estimated

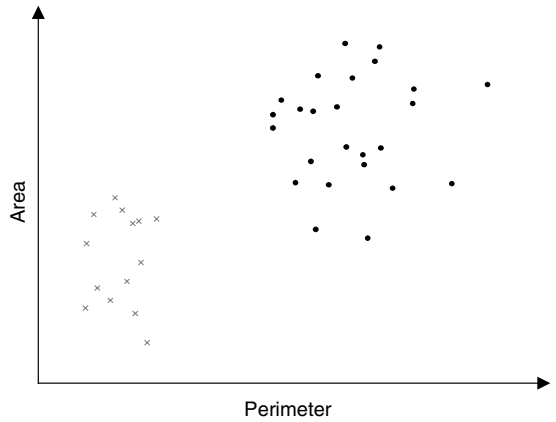

Figure 3. Characterization of two hypothetical classes of neural shapes in the area/perimeter feature space. The similarity between cells from the same classes and dissimilarity of cells from different classes frequently lead to the respective neurons being described as defining 'clouds' or clusters in the feature space.

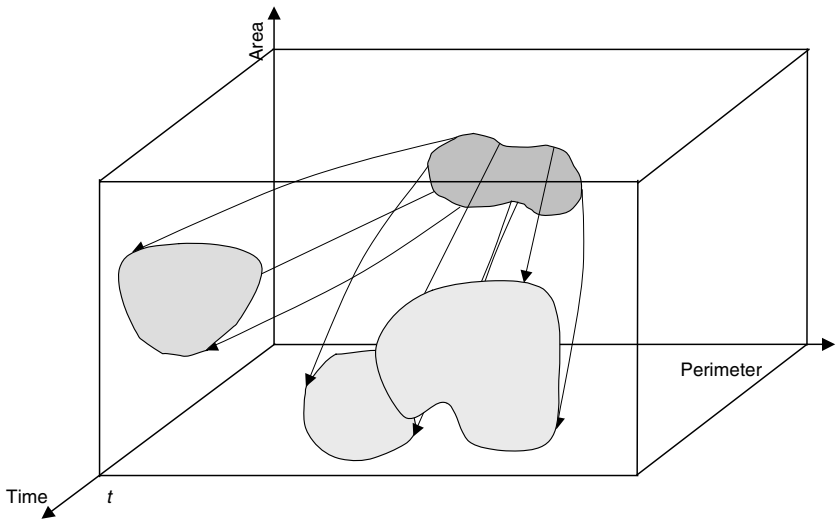

Figure 4. The process of nerve cell differentiation can be properly represented graphically in terms of the concept of potential space of a specific type of precursor cell.

by using some numerical computational approach. As could be expected, the possible vectors $\vec{S}(\vec{p}) = [\text{perimeter, area}]^T$, illustrated in figure 1(b), tend to form a cloud of varying density in the respective phase space. Now, if we divide the phase space into regular bins, and count the number of observations inside each of such bins and divide this number by M, we obtain a relative frequency histogram. The density probability function is obtained as the size of the bin is reduced to an infinitesimal, as the number of samples is taken to infinity. One of the important properties of this function, henceforth indicated as D, is that the chance of observing a neuron with measures inside a specific feature interval is given by equation (1), where P is the perimeter and A is the area, in this particular case:

$$D(P_1 \leqslant P < P_2,\ A_1 \leqslant A < A_2) = \int_{P_1}^{P_2} \int_{A=A_1}^{A_2} q(P, A)\, \mathrm{d}P\, \mathrm{d}A. \tag{1}$$

In fact, the density probability function provides all possible information about the statistical behaviour of the data, being therefore a complete stochastic model. While the evolution of density probability functions in specific situations can be modelled by differential equations (for instance, random walk processes lead to the Fokker–Planck formulation [21], which is basically a diffusion differential equation), these functions can also be directly used as a basis for classification, which can be achieved by using Bayes decision theory [22]. Another interesting possibility is to apply dynamical system concepts and tools [23], such as the use of the Lyapunov coefficient to characterize the sensitivity of environmental effects over shape trajectories.

3. Geometrical measures for neural shape characterization

This section presents the main motivation and guidelines underlying the integrated multiscale approach to neuromorphology reported in this paper, which follows the developments reported in [20]. It addresses the need to have an effective and comprehensive set of geometrical measures while taking advantage of the multiscale paradigm.

While a larger number of measures allows a more comprehensive characterization of the shape, eventually leading to a complete representation, the complexity and computational demands resulting from using a large number of measures tends to increase substantially, in such a way that only the smallest number of measures capable of providing the required information should be considered. Indeed, an interesting question that has been posed in the literature [24, 25] regards the identification of the smallest number of measures that would allow us to represent a specific class of nerve cells. While the length of dendritic and axonal segments and the angle at branch points no doubt provide important geometrical information to be used in neuronal characterization, the above question is complicated by the fact that physical, chemical, and mechanical properties of the membrane and cell dynamics, including electrochemical activity and interaction between neighbouring cells, should necessarily be related and incorporated in some way into the sought representation. Yet, while the issue of minimal representation of neural shape remains a challenge, it is also important to observe that several problems in neuroscience can be suitably addressed while limited to characterization. Such situations include the characterization of the surface of contact between the cell membrane and the extracellular medium and the study of the orientation of nerve cells, among many others, and provide the main situation considered in the present paper.

For such reasons, the choice of a suitable set of geometrical measures defines an important issue underlying many investigations in neuroscience. Basically, there is an infinite number of possible morphological measures at the same time as there are no clear-cut rules or procedures for selecting them. Therefore, in practice the selection of measures is determined by the issues being addressed in each specific investigation, previous knowledge of the problem, and previous experience with neuromorphology. Of special relevance is knowledge about the potential of each measure to express specific biologically relevant properties. Indeed, although several approaches have been considered for neuromorphological characterization (e.g. [26–35]), there are few standardized neuromorphological measures in the literature. Ideally, it would be interesting to have a set of versatile, simple, and meaningful geometrical measures for neural shape characterization which could be applied to a large number of problems in neuroscience. The current work proposes that this can be achieved by considering four families of measures, based on differential geometry, symmetry axes, influence area, and complexity. Although exhibiting some interesting interrelationships, these measures, which include some recently introduced concepts and methods, can provide a comprehensive (often complete) characterization of relevant geometrical properties of the cells, as discussed in the

Table 1. The three families of morphological measures and, in each case, the main potential for neural geometry characterization.

	Potential for geometrical characterization	
Family of measures	Isolated	Ensemble
Differential geometry	• Arc length • Curvature • Orientations (tangent field) • Contour segmentation and branch point identification	
Symmetry axes	• Hierarchical representations (dendrograms) • Number of branches • Number of hierarchies • Angles and lengths of processes	
Complexity	• Multiscale fractal dimensions • Area of interface between cell membrane and extracellular medium • Surface of contact • Influence area	• Surface of contact

following sections. Another important aspect of the proposed approach is that all the measures considered exhibit a multiscale nature, allowing not only the selection of specific scales relevant to each problem considered, but also the enriched characterization of neural geometry along several spatial scales. Table 1 presents each of the families of measures considered and the main respective potential for geometrical characterization.

Figure 5, to be considered in the following sections, presents the basic steps and data dependence involved in the implementation of the four families of measures, starting from the raw image (e.g. those acquired from a microscope). Data and processes are represented by boxes and arrows, respectively.

4. Image acquisition and pre-processing

The process of characterizing neuronal shape starts with the acquisition of digital images. This is typically done either by using an optical transmission/fluorescence microscope, producing 2D images captured by simple cameras, or by using more sophisticated technologies such as confocal imaging systems, where a series of slices are obtained directly from the histological slides and later merged into fully 3D structures. In both cases, the nerve cells or structures have to be separated from the background or other secondary structures, a process technically known as *segmentation*. This task is complicated by noise and other artifacts frequently present in the acquired data, which has precluded a fully automated approach. In the case of 3D imaging, once the structures of interest are segmented, additional processing has to be applied in order to properly integrate the 2D segmented data into 3D reconstructions [36–39], or do the segmentation directly from the 3D stack of images [40].

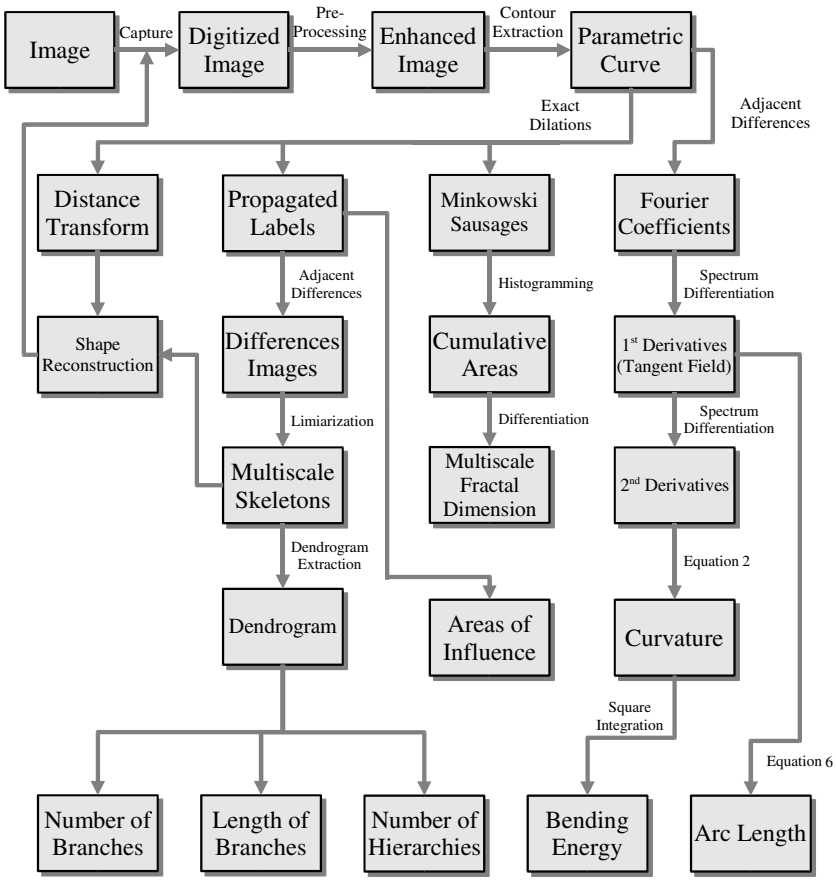

Figure 5. The main data (boxes) and processes (arrows) underlying the currently reported framework for neural geometry characterization.

5. Differential geometry measures

Most of the mathematical concepts and tools used in science, especially in physics, rely on differentiable functions and fields defined along continuous spaces, as required for the use of the differential equations. Indeed, as implied by the Taylor series, the several derivatives of signals provide a comprehensive characterization of its properties around a small neighbourhood (actually an exact representation, provided all the infinite derivatives are taken into account). The systematic study of derivatives and their combinations into meaningful measures is the main objective of differential calculus which, given its long and extremely successful tradition, provides a most valuable source of concepts and methods for shape analysis and neuromorphology. While the standard derivatives generally vary when the signal is translated, rotated, or subjected to some other geometrical transformation, some measures obtained through special combinations of derivatives provide several types of invariance. For instance, the curvature [41, 42] of 2D curves, defined by equation (2), is invariant under translation and rotation:

$$k(t) = \frac{\dot{x}(t)\ddot{y}(t) - \dot{y}(t)\ddot{x}(t)}{(\dot{x}(t)^2 + \dot{y}(t)^2)^{1.5}}. \tag{2}$$

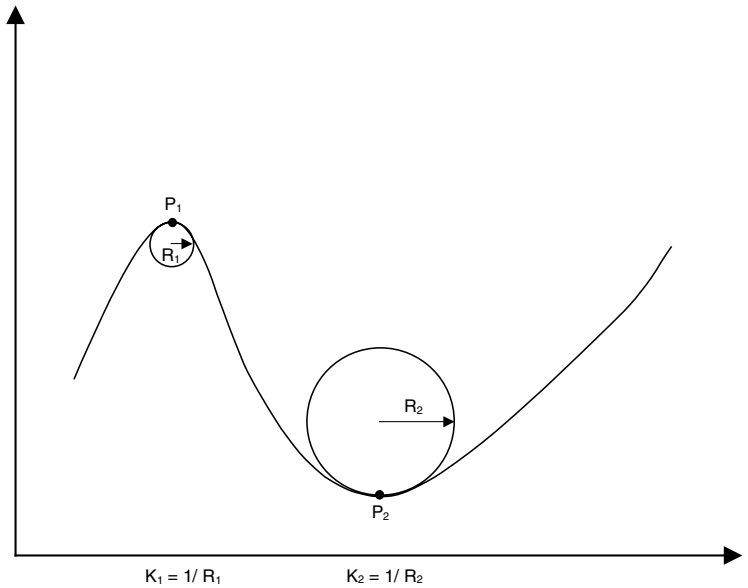

Figure 6. The curvature at any specific point P along a curve can be understood as the inverse of the radius of the osculating circle, i.e. the circle that has three points of contact with the curve.

The curvature also provides a complete representation up to translation and rotation, in the sense that the original curve signals ($x(s)$ and $y(s)$) can be recovered, up to translation and rotation, from the respective curvature signal $k(u)$ by using equations (3):

$$\begin{aligned} \theta(s) &= \int_0^s k(u)\,\mathrm{d}u + \theta_0 \\ x(s) &= \int_0^s \cos\theta(u)\,\mathrm{d}u + x_0 \\ y(s) &= \int_0^s \sin(u)\,\mathrm{d}u + y_0. \end{aligned} \tag{3}$$

In addition to such powerful features, the curvature also allows clear conceptual and geometrical interpretations [20, 33]. While the curvature provides a measure of the local change of orientation of the tangent to a curve, it can also be understood in terms of *osculating circles* (see figure 6). Given a point of the curve, the respective osculating circle is defined as the circle that touches the curve at three infinitesimally spaced points (e.g. [42]). The curvature absolute value can be verified to be equal to the inverse of the radius of this circle. Finally, the sign of the curvature provides valuable indications about the concavity of the local portion of the shape, in such a way that points of the curve where the curvature sign changes (*inflection points*) can also be considered as especially important organizing features of the curve.

For all the above reasons, special attention has been focused on curvature as a powerful resource for shape analysis (e.g. [43, 44, 46]). The main problem of applying curvature to shapes represented in digital images arises from the spatially quantized (or discrete) nature of such signals. This shortcoming has been naturally circumvented in the approach reported in [45, 46], where the Fourier transform, combined with a Gaussian smoothing filter, is used to interpolate between the points of discrete shape contours. The combined use of the Fourier transform and Gaussian smoothing for curve interpolation provides an effective

means for reducing the small-scale, and consequently high-frequency, non-uniformities, anisotropies, and noise implied by the spatial sampling of the curves [47, 48]. In addition, the non-uniform spacing along subsequent contour elements is properly dealt with by the fact that the curvature expression adopted, equation (2), is inherently suitable for non-uniform parametrization [41]. The use of the Fourier transform confers a series of advantages. First, the Fourier transform provides an orthogonal and highly uncorrelated representation of the contour, implying that the Fourier transform coefficients are in themselves highly effective as a complete curve representation [49–51]. Second, as they are widely adopted in signal processing and communications, high-speed algorithms—and even integrated circuits—can be found that are capable of performing the fast Fourier transformation of thousands of points in a matter of a few microseconds. Moreover, the use of the Fourier spectral representation, where the 2D contour is represented in terms of a linear combination of smooth functions (complex exponentials), provides a natural and accurate means to numerically estimate the first and second derivatives implied by the curvature definition in equation (2). In addition, the Gaussian filter naturally introduces a spatial scale parameter, namely the standard deviation σ, which endows the method with multiscale capabilities. The first and second derivatives of the x-signal (analogous results are obtained for the y-signal) required by the curvature definition in equation (2) are obtained as indicated by equations (4) and (5), where f is the frequency $\Im$ in the Fourier transform, and $g_\sigma(t)$ is the normalized (unit-area) Gaussian function with standard deviation σ. In other words, the x- and y-signals are convolved with the same smoothing Gaussian filter, which can be done more effectively in the frequency domain. We have

$$\dot{x}(t) = \Im^{-1}\{(\mathrm{i}\,2\pi f)\Im\{x(t)\}\Im\{g_\sigma(t)\}\} \tag{4}$$

$$\ddot{x}(t) = \Im^{-1}\{-(2\pi t)^2\Im\{x(t)\}\Im\{g_\sigma(t)\}\}. \tag{5}$$

The estimated first derivative provided by equation (4) can be immediately used to calculated the arc length of the curve, which is done by using equation (6):

$$L|_{a\to b} = \int_a^b \sqrt{\dot{x}^2 + \dot{y}^2}\,\mathrm{d}t. \tag{6}$$

Figure 7 presents an example of the spectral approach to curvature estimation, applied through numerical implementations of the above methodology involving the discrete Fourier transform (see [20,46]). The shape in this example has been artificially constructed in order to best illustrate the concepts and processing stages. The original shape in (a) is first edge detected and contour followed, producing the contour in (b) which is then represented as the pair of 1D signals in (c), corresponding to the x- and y-coordinates along the arc length parametrization. The curvature obtained for $\sigma = 10$ is illustrated in (d) and (e).

The potential of curvature for neuronal shape characterization stems directly from the completeness and powerful features of this measure, especially the fact that it is invariant under translation and rotation. For instance, the curvature can be used to effectively identify the branches and terminations of neural processes, which correspond to curvature peaks. In addition, statistical characterizations (e.g. histogram or moments) of the curvature value distribution along a cell or one of its portions can provide valuable information about the smoothness of the membrane geometry, in the sense that a smoother membrane will produce lower curvature values. Another interesting possibility defined by the spectral approach to differential geometry relates to the accurate numerical estimation of the arc length of neural processes, a possibility that is illustrated in section 8.3. Other measures arising from differential geometry include the tangent and normal fields, and in the case of 3D shapes maximum and minimum curvature, mean and Gaussian curvature, parabolic lines and umbilical points, to name but a few [41].

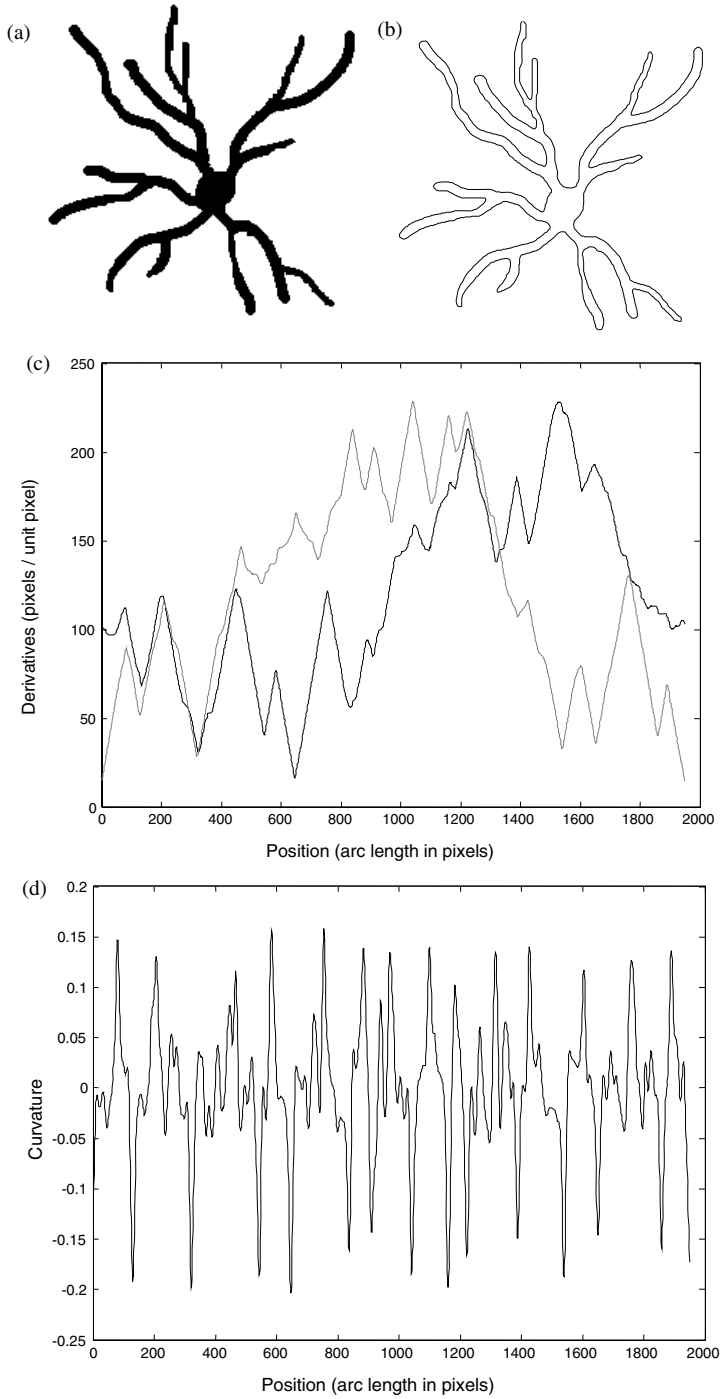

Figure 7. An example of spectral curvature estimation: original neural shape (a); respective edge detected version (b); contour representation in terms of the 1D x- and y-signals (c); and the curvature obtained for $\sigma = 10$ shown as a one-dimensional signal (d) and superposed onto the original shape (e). In part (e), negative values occur at the ends of branches and positive values in the forks between branches (this part is in colour in the electronic version).

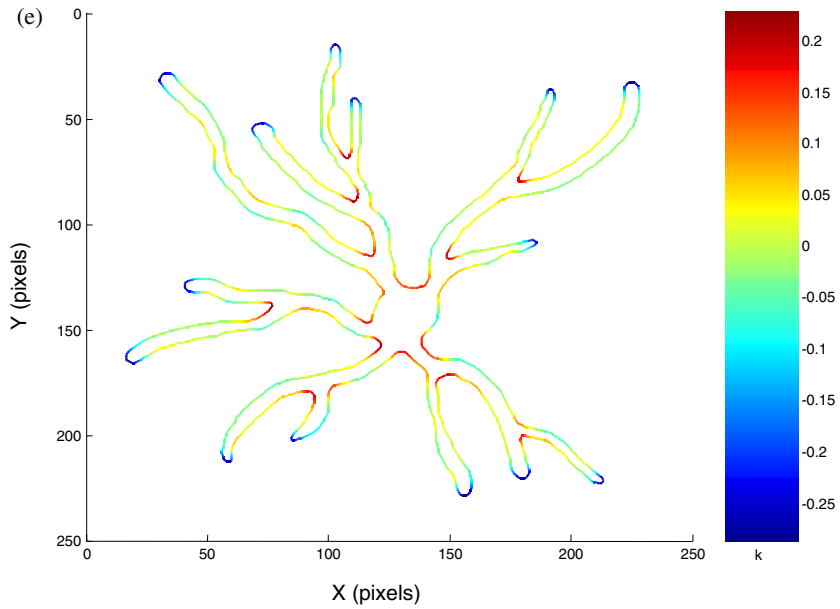

Figure 7. (Continued.)

6. Symmetry axes and skeletons

Symmetry is one of the most important measures characterizing organisms, possibly because it may simplify the instructions for producing shapes and support certain types of behaviour and function. One of the most comprehensive characterizations of shape symmetries can be achieved by using the concept of symmetry axes, which are also known as skeletons [52, 53]. One of the most popular and natural types of symmetry axis, the medial axis of a 2D shape, is defined as the centre of all possible circles that are maximally inscribed in the shape [41]. Such skeletons are fully connected and have a tree as inherent structure, which provides a suitable characterization of the hierarchy of the shape under analysis. Two types of skeleton are usually defined by the contours of a 2D shape: the *internal*, corresponding to the skeletons inside the shape, and *external*, falling outside the shape. Basically, while internal skeletons are produced by convex portions of the shape, external skeletons are induced by shape concavities. In addition, each skeleton termination can be associated with a peak of curvature along the curve [54].

When combined with the distance transform of the shape, namely the process of assigning to each point around the shape the smallest distance between it and the point, the medial axis provides a complete representation of the shape, in the sense that it can be fully recovered. While traditional medial axes are known to be unstable with respect to small shape perturbations, in the sense that any small bump in the shape will produce a new skeleton segment, stable multiscale skeletons can be obtained by using the approach described in [55, 56]. That approach involves assigning successive integer numbers—hence labels—to adjacent pixels of the shape contour, propagating these labels by using exact distances [55], and taking the differences between the labels of four adjacent pixels.

The result of such processing is a difference image that can be subjected to a threshold operation in order to produce a multiscale characterization of the shape, as illustrated in figure 8.

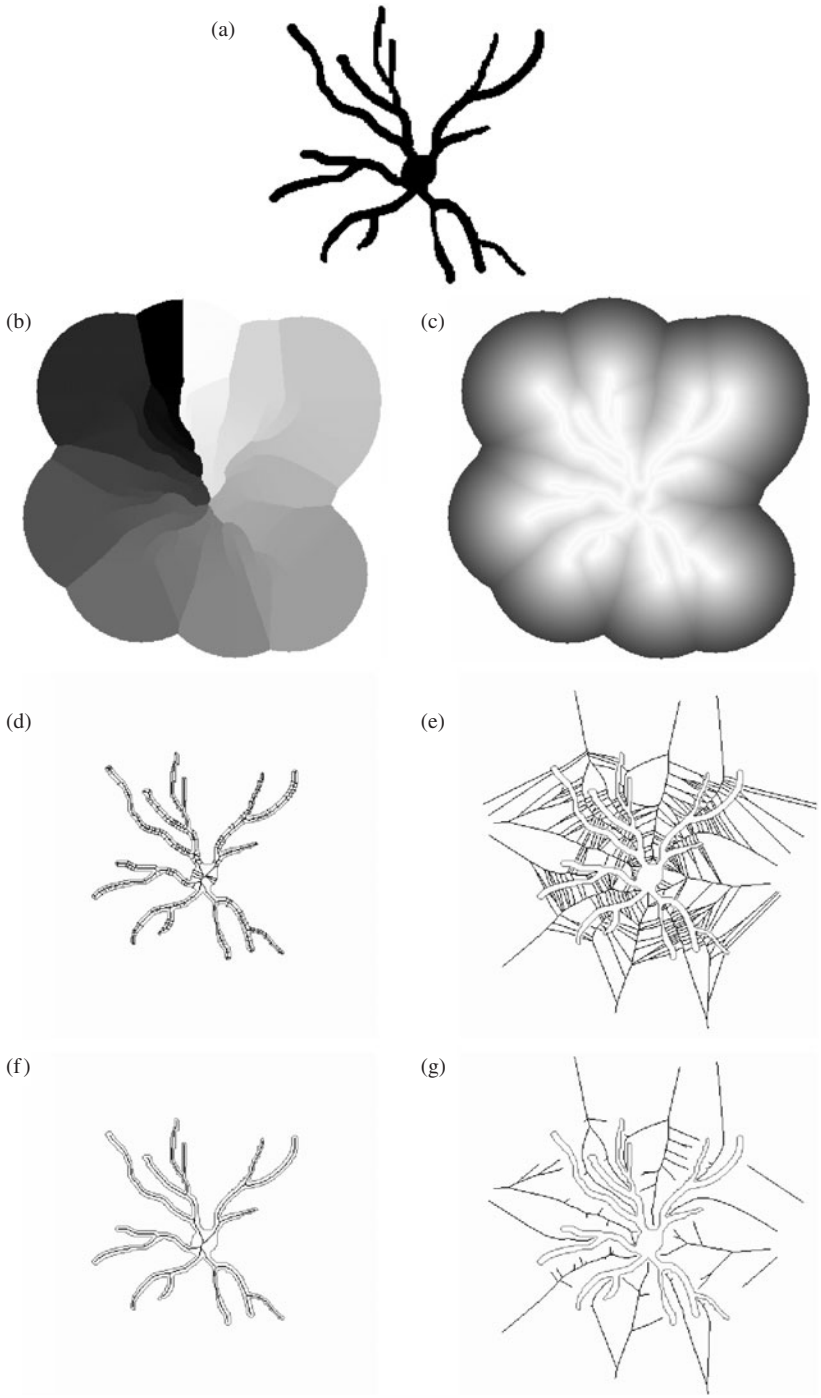

Figure 8. Multiscale medial axes extraction: original neural shape (a); propagated labels (b); distance transform (c); and internal and external medial axes obtained for a threshold $T = 2$ ((d), (e)); 5 ((f), (g)); 50 ((h), (i)); 100 ((j), (k)) and 300 ((l), (m)).

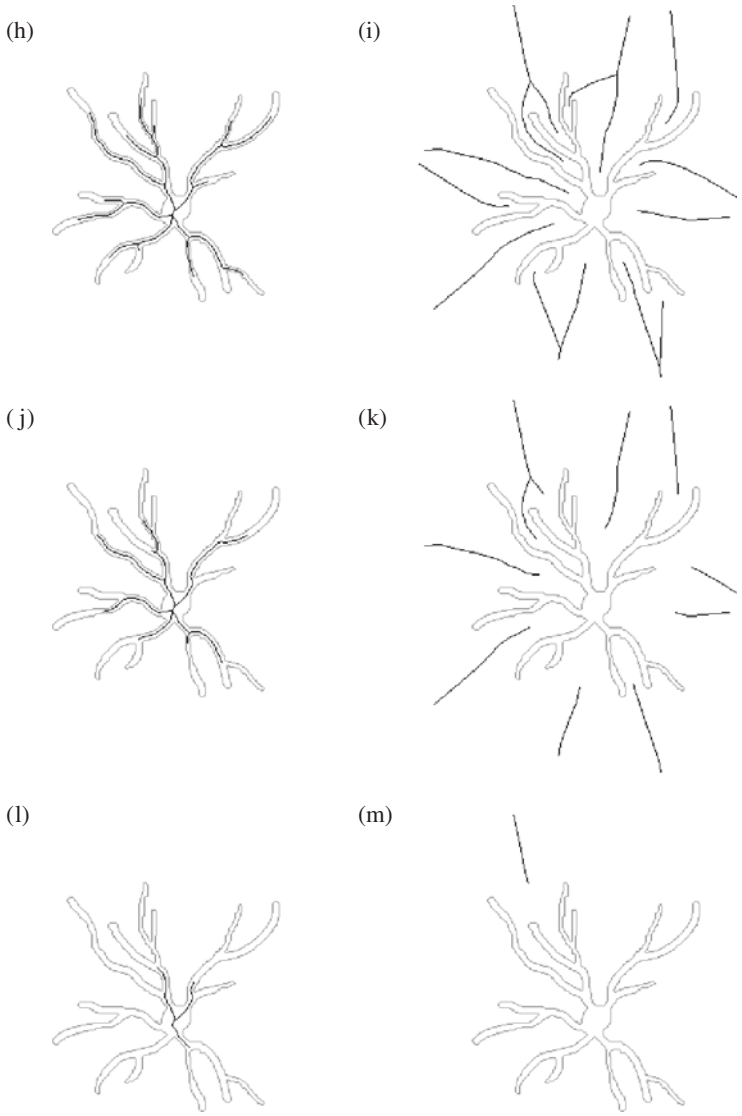

Figure 8. (Continued.)

This figure shows the original neural shape (a), the propagated label, where each label value is represented by a grey-level (b); the distance transform (c); and the internal and external skeletons obtained for $T = 2$ ((d), (e)); 5 ((f), (g)); 50 ((h), (i)); 100 ((j), (k)) and 300 ((l), (m)). Higher threshold values will produce simplified (pruned) versions of the skeletons, which can be combined with the respective distance transform in order to produce filtered versions of the shape. This type of non-linear filter has the interesting property of eliminating small-scale detail while not disturbing higher-scale portions of the shape [57]. A particularly effective approach for implementation of the above-mentioned multiscale skeletons has been described in [58]. The choice of the most suitable scale depends on each specific problem. For instance, if one is interested in characterizing small-scale detail, the threshold should be as low as possible. On the other hand, and as is more frequently required, the threshold is selected just as high as

necessary to remove details implied by the object spatial sampling (e.g. the jittered outlines of digital curves) without removing relevant geometrical properties of the shape. According to the latter criterion, the skeleton shown in figure 8(f) represents possibly the best compromise.

Symmetry axes can be used to extract the hierarchical structure underlying all nerve cells, from which dendrograms can be immediately extracted (see example in section 8.1). In addition, granulometric information expressing the distribution of widths along the neural processes cells can be obtained in terms of histograms of the distance values verified along the symmetry axes. A number of additional relevant geometrical features can be extracted from skeletons, including the number of hierarchies, number of branch points, histograms of segment lengths, and branch angles.

7. Complexity

Although subjective, morphological complexity is an important attribute of neurons. Two effective means for complexity characterization, allowing objective interpretations, are described below.

7.1. Multiscale bending energy

The bending energy, directly proportional to the sum of squared curvature values, provides an indication of the energy stored in a specific shape [59]. Thus, while a straight line presents zero energy, a more intricate contour will present higher bending energy than a smooth one. A multiscale version of this measure can be obtained directly from the multiscale curvature by using equation (7), applied to the Gaussian smoothed contours (equations (4) and (5)), providing additional information about how the energy evolves as the shape is smoothed out:

$$\varepsilon_\sigma = \sum_{i=1}^{N} k_\sigma^2(i). \tag{7}$$

Figures 9(c) and (d) present the multiscale bending energies for the neural contours in (a) and (b), respectively.

7.2. Multiscale fractal dimensions

The fractal dimension provides a quantitative characterization of the complexity of curves as induced by self-similarity. This concept can be better understood through the following example with respect to the Koch triadic curve, which is obtained by replacing every straight-line segment of the basic pattern shown in figure 10(a) by itself, *ad infinitum* towards both the microscopic and macroscopic spatial scales. The fractal dimension F of this curve is calculated as in equation (8), where S is the arc length of the basic pattern and L is the distance between the two extreme points of the basic pattern:

$$F = \frac{\log(S)}{\log(L)} = \frac{\log 4}{\log 3} \simeq 1.26. \tag{8}$$

Therefore, the fractal dimension provides a nice indication of how much the curve extends itself through space. As a consequence, more intricate curves will cover the surrounding space more effectively, leading to higher fractal dimensions. Observe that $F = 1$ when the basic pattern is a straight line, which corresponds to its topological dimension. Despite the good potential of this measure to characterize complexity in a more objective fashion, its extension to real objects is complicated by the fact that the latter are not perfectly self-similar. In fact,

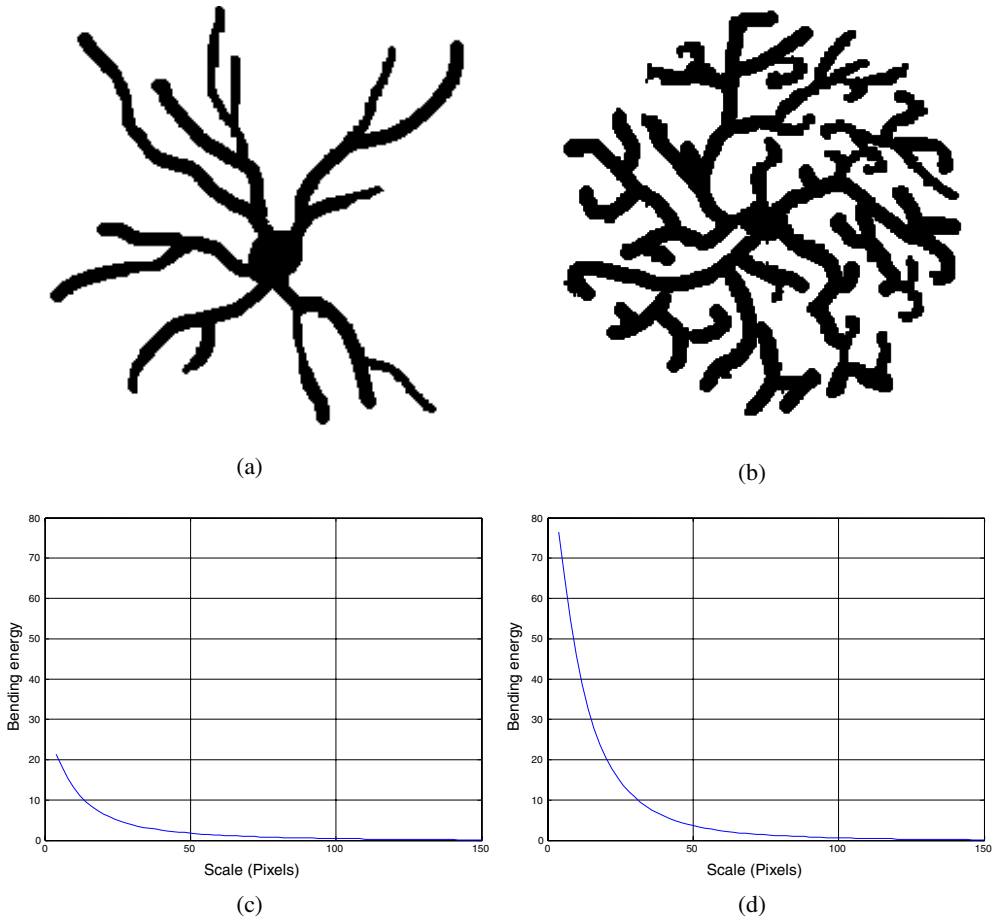

Figure 9. The bending energy can be used to characterize, in an objective fashion, the complexity of parametric contours of neuronal cells and structures, in the sense that the higher the bending energy, the more complex the shape. Good results have been obtained when using the bending energy for the purpose of classifying nerve cells [30].

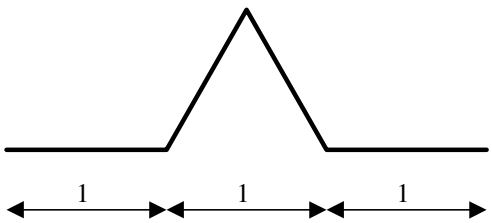

Figure 10. The basic pattern used to generate the Koch triadic curve.

only a few orders of similarity are usually found for natural objects, such as the three or four orders found in fern leaves. Indeed, the fractality of such objects, especially when represented in digital images, is limited at both microscopic and macroscopic scales. First, for scales smaller than the image resolution, the fractal dimension tends to zero, the dimension of the image pixels. On the other hand, for scales larger than the object, the respective dimension

tends to zero, as the object tends to behave as a point for large distances. Therefore, real objects will present higher fractal values only along limited intervals of spatial scale. This problem can be suitably addressed by using the multiscale extension of the fractal dimension recently described in [60], which involves the numerical estimation of the first derivative of a log–log cumulative function, more specifically the graph of the logarithm of the dilated area in terms of the logarithm of the spatial scale (i.e. radius of the dilating discs). This extension involves obtaining not a scalar value of fractal dimension as usually done, but expressing a fractal function in terms of the spatial scale that properly reflects the behaviour of the object when observed at different magnifications. Therefore, the multiscale fractal dimension represents a less degenerate geometric characterization, in the sense of preserving more information about the geometry of the original object. The numerical process for estimating the multiscale fractal dimension is explained in the following with respect to the Minkowski sausage approach.

Given the contour of a shape, its *Minkowski sausage* with radius R can be obtained as the union of all balls of radius R centred at each of the contour points. Such sausages can be obtained by using the same dilation procedure adopted for producing the multiscale skeletons described in section 6. Thus, given the contour of a shape, a log–log function can be obtained by considering the logarithm of the Minkowski sausage areas in terms of the logarithm of the radii considered. The derivative of this log–log function produces the multiscale fractal dimension, which is a function of the logarithm of the spatial scale represented by the radii. Figure 11 illustrates this approach with respect to simpler (a) and more complex (b) neural shapes. The respective log–log graphs are given in (c) and (d), whose multiscale fractal dimensions, obtained in terms of the respective derivatives, are shown in (e) and (f).

It is clear from this example that the multiscale fractal dimensions obtained exhibit higher values only along a limited extent of the spatial scale. As such graphs indicate the fractal behaviour of the contour in terms of the spatial scales, a much more comprehensive characterization of the shape complexity is obtained than by using a single fractal dimension obtained by linear interpolation through the log–log function, as done conventionally (e.g. [61]). The following three particularly meaningful features can be extracted from the multiscale fractal dimension graph: (a) the maximum fractal value, which indicates the maximum complexity of the contour; (b) the length of the spatial scale interval along which the curve exceeds a specific value, which is proportional to the number of hierarchical self-similarities in the shape; and (c) the area of the graph (called the total complexity) divided by the maximum fractal value (the division is necessary for normalization and decorrelation), which gives an overall idea of the shape complexity. Another useful measure is the median (i.e., the middle value of a set of values) of the multiscale complexity. Figure 12 presents a set of simple real nerve cells (1–4) and a set of more complex nerve cells (5–10) and the feature space obtained by the respective maximum and total fractal dimension. The potential of this pair of measures for discriminating between these two types of cell is evident.

8. Application examples

8.1. Automated dendrogram extraction

This section describes how the multiscale skeletonization approach described in section 6 can be used as an effective means to obtain dendrograms from 2D digital images of real nerve cells. It should be recalled that the dendrogram represents the data structure containing the geometrical information required by most neural simulation approaches, which includes the extension of each process and the hierarchical branching structure. The procedure is illustrated with respect to the neuron in figure 13, and assumes the skeleton in figure 8(f) has already

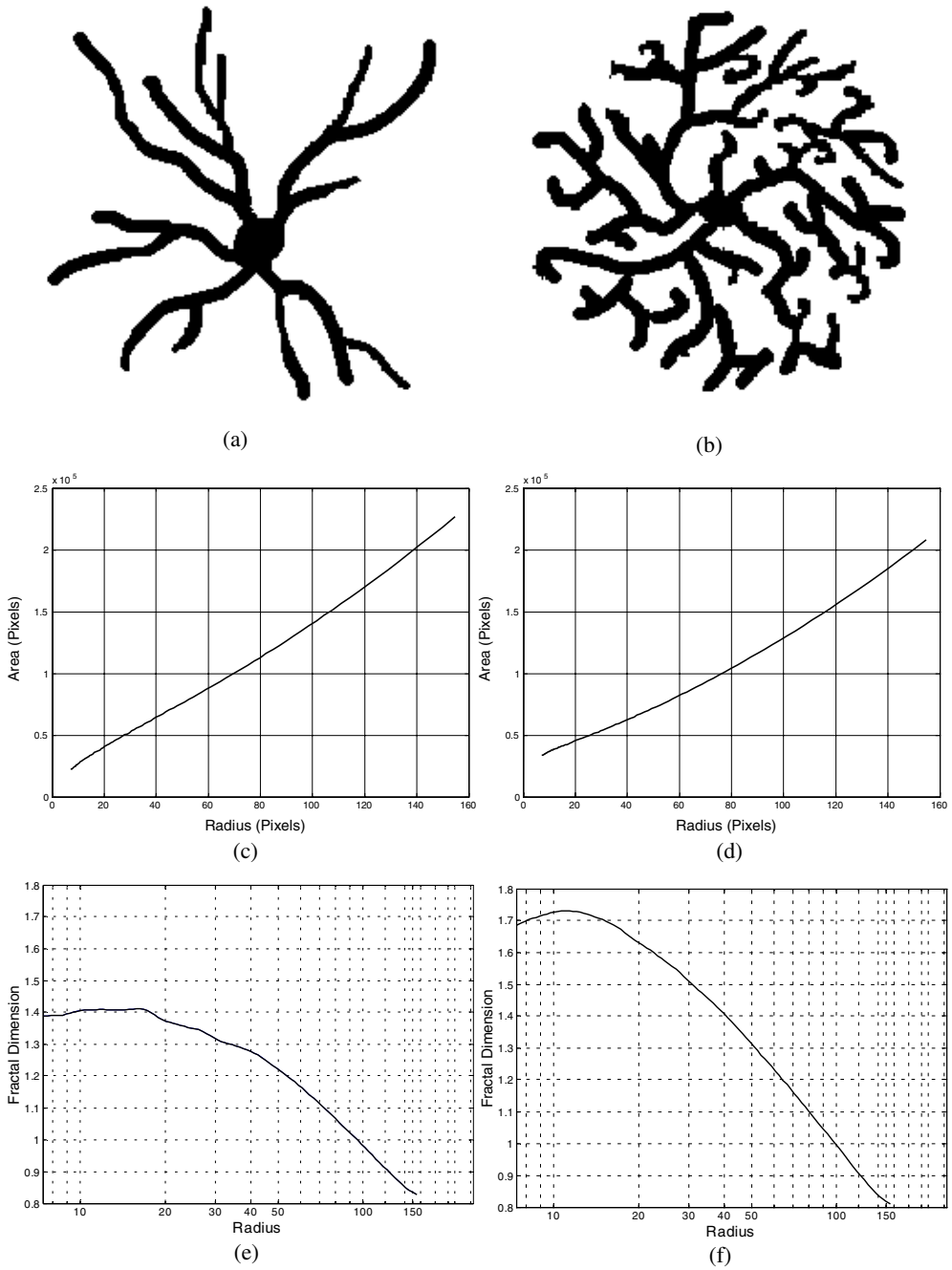

Figure 11. A simpler (a) and a more complex (b) shape and their respective log–log functions ((c), (d)) and multiscale fractal dimensions ((e), (f)).

been calculated as described in section 6. Given such a skeleton, a simple algorithm is applied that, starting from the soma centre, follows the skeleton structure while storing into a queue the coordinates of every observed branching point. The structure obtained can subsequently be used to produce the dendrogram tree structure.

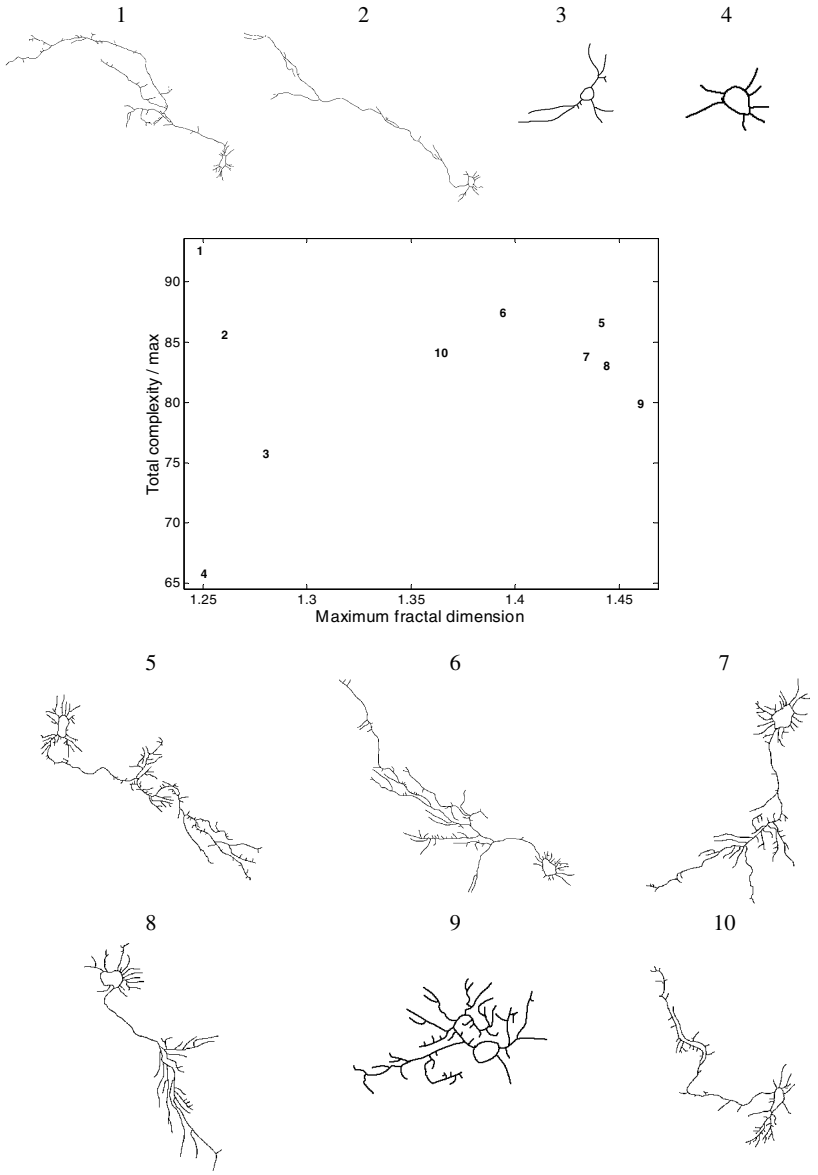

Figure 12. Simple (1–4) and more complex (5–10) real nerve cells and the respective feature space defined by the median and maximum values of the fractal dimensions.

8.2. Characterization of neurodevelopmental alterations underlying mental retardation

This section illustrates the application of the multiscale fractal dimension to characterize the complexity of cultured neurons transfected with a gene involved in mental retardation. Mental retardation is characterized by a global deficit in cognitive functioning (intelligence quotient (IQ) below 70) and an onset during childhood. Golgi studies conducted three decades ago showed that mental retardation is associated with a decreased complexity of the dendritic trees of cortical pyramidal neurons, a lowered density of dendritic spines, and abnormalities

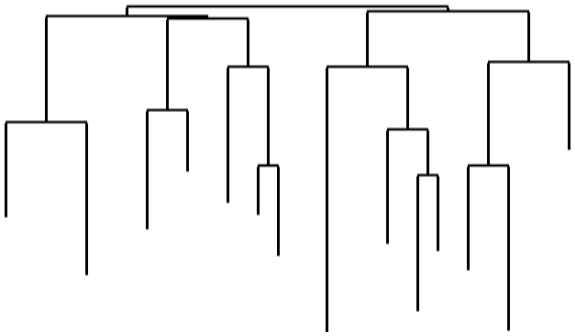

Figure 13. The dendrogram of the neural shape in figure 8(a), obtained by following the skeleton in figure 8(f).

in spine shape. Since spine synapses mediate most of the excitatory synaptic transmission and dendritic complexity is a major determinant of information processing at the single-neuron level, these findings suggest that at least some forms of mental retardation may be due to abnormalities in the development of neuronal morphology and/or connectivity. Spine morphology has a strong influence on the transmission of synaptic signals to the dendritic tree and spines are considered to be focal points of synaptic plasticity underlying learning and memory. Thus, spine deficiencies may indicate disturbances in learning and memory as an additional cause of mental retardation [62].

Recent clinical genetic studies have led to the cloning of seven mutated genes which cause non-syndromic mental retardation [63]. Three of these genes are involved in cellular signalling through Rho family GTPases. Rho GTPases regulate the dynamics of the actin cytoskeleton and neuronal morphogenesis and connectivity, also in response to synaptic activity [64, 65]. Abnormal Rho GTPase signalling may therefore alter neuronal network development and/or plasticity [65], resulting in deficient neuronal information processing. We investigate how the Rho-linked mental retardation genes alter neuronal morphogenesis and connectivity. One of these genes, OPHN1, encodes for oligophrenin-1, which inhibits one of the Rho GTPases, possibly RhoA [66]. Mutations in OPHN1 are expected to increase signalling through RhoA. When such mutations result in reduced complexity of dendritic trees, we expect overexpression of wild-type oligophrenin-1 to increase morphological complexity. Overexpression was induced by transfecting wild-type human OPHN1 into cultured neurons of foetal rat cerebral cortex in a 2D tissue culture system [67] at two days. Morphological analysis of axons and dendrites was performed at four days. As a positive control for RhoA inhibition, neurons were also transfected with p190 RhoGAP, the prototypic GAP for RhoA [68]. Transfected neurons were identified by immunostaining for β-galactosidase (encoded by lacZ), which was cotransfected with OPHN1. Since β-galactosidase, a cytoplasmic protein, fills the entire neuron, the β-galactosidase staining was also used to delineate the morphology of the neurons. Neurons transfected with OPHN1 or a control vector were recorded at random in a blind manner, using a Zeiss LSM410 confocal microscope at a resolution of 0.30 μm/pixel, and manually traced in Corel Photopaint (version 9.0).

Figure 14 illustrates several rat cerebral cortex neurons from control transfected neurons and the respective characterization in terms of median and maximum values of the multiscale fractal dimensions. Figure 14 presents the feature space obtained for all cerebral cortex neurons, where circles, crosses, and dots represent control, oligophrenin-1, and Rho-GAP transfected cells, respectively. The substantial overlap between the three types of cell through

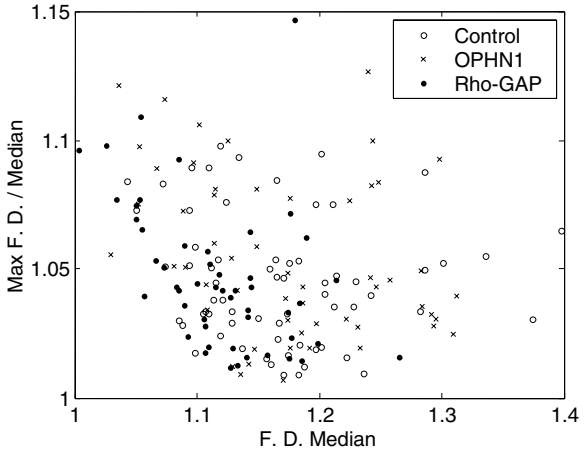

Figure 14. The distribution of the three types of cell considered in the features space defined by the median and maximum fractal values.

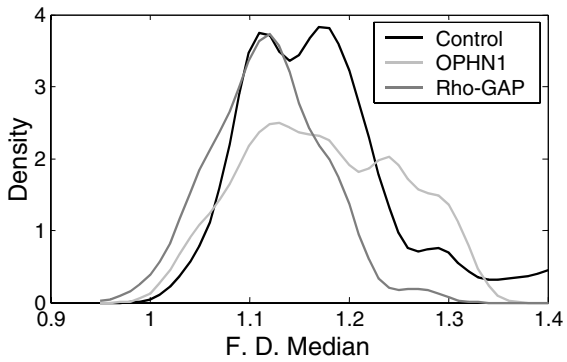

Figure 15. Histograms of the median fractal dimension values for the three types of cell considered. The oligophrenin-1 type clearly presents the widest dispersion.

the feature space considered clearly indicates that control and oligophrenin-1 overexpressing neurons cannot be clearly distinguished in this feature space. On the other hand, RhoGAP transfected neurons tend to be clustered towards the lower values of the median and maximum values of the multiscale fractal dimensions. As shown in figure 15, histograms obtained for the median of the fractal dimensions indicate distinct distributions for the three types of cell. While the oligophrenin-1 overexpressing neurons more broadly dispersed towards higher values, the RhoGAP overexpressing neurons show a narrower distribution at lower values. Assuming mass equiprobability (i.e. that the neurons have similar densities), and according to Bayes classification methodology [22]—i.e. considering the maximum values along the histogram x-axis, the geometrical complexity of the cells would increase from the RhoGAP to the oligophrenin-1 overexpressing neurons, with the control neurons in between. With regard to oligophrenin-1, these observations are in agreement with our expectations about the involvement of oligophrenin-1 in mental retardation. However, p190 RhoGAP overexpression (which should decrease endogenous RhoA activity) did not increase complexity. This is surprising, as expression of activated RhoA reduced dendritic complexity in hippocampal neurons [69]. On the other hand, expression of dominant-negative RhoA (which inhibits the

activity of endogenous RhoA) also did not affect dendritic complexity in hippocampal neurons, which may indicate that in these neurons RhoA is not activated under normal growth conditions.

Further investigations will be required to determine whether the effect of oligophrenin on neuronal complexity is related to its presumed function as an inhibitor of RhoA. In addition, complexity as measured here is a composite parameter describing neuronal morphology, which may be affected differentially by alterations in different aspects of neuronal morphology. Subsequent studies should validate how complexity relates to other measures of neuronal morphology such as numbers of neurites, numbers of branches, and numbers of segments.

8.3. Growing axons

The geometrical characterization of the growth of axons provides an important starting point for understanding this important and not yet well-known process. One of the most relevant morphological measures to be considered in such analysis is the *arc length* defined between the axon terminations and some reference point, usually the position where the axon emerges from the soma. In addition, it is also important to quantify the *velocity* of the arc length evolution. The spectral approach to differential geometry described in section 5 provides a natural and accurate means for estimating automatically the arc length between two points a and b along a parametric curve, which is done by using the first contour derivatives, as given in equation (6).

This methodology has been applied to movies of growing axons. Cerebral cortex neurons from 18-day foetal rats were grown in a serum-free medium and recorded at 10 min intervals with phase contrast optics at a resolution of 0.825 μm/per pixel. The recorded neuron used here started with a single unbranched axon which grew out in a saltatory manner, typical for developing neurons. At different time points the axon produced two side-branches, which appeared to elongate in an alternating fashion. Often, when one branch was elongating, the other stopped or slowed down. These observations suggested that elongation of different branches along the same axon does not occur independently, and may be subject to competitive mechanisms.

Figure 16 illustrates eight successive frames of the growing sequence. After extracting the parametric representation of the contours, which has been done by applying a standard contour-following algorithm [20], the respective first derivatives are obtained and substituted in equation (4), yielding the arc length evolution shown in figure 16. The corresponding arc length velocity, obtained by using standard finite-difference methodology, is shown in figure 18(a). Each of the three branches in these two figures, labelled 1, 2, and 3, corresponds to the birth of a new axon segment. Such a pair of graphs provides a clear and precise characterization of the arc length evolution through time. For instance, it is clear from figure 17 that the axon segment 1 remained longer than 2 and 3. On the other hand, axon segment 3 overtook 2 at time 2500 min. It is also evident that all segments experienced arc length retraction, identified by decreasing arc length values in figure 17 and negative velocity values in figure 18(a). Particularly remarkable is the high velocity increase (i.e. acceleration) exhibited by axon segment 3 starting from time 2100 min. It appears that in particular the acceleration parameter is an excellent indicator of the antagonistic behaviour of the different branches (figure 18(b)), suggesting a strong correlation in the outgrowth rate of different axon segments of the same neuron. Finally, figure 19 shows the shape trajectory obtained by considering all three measures.

9. Concluding remarks

This article has reported an integrated and systematic approach to automated neuromorphometry. Relying strongly on sound mathematical principles and effective computational

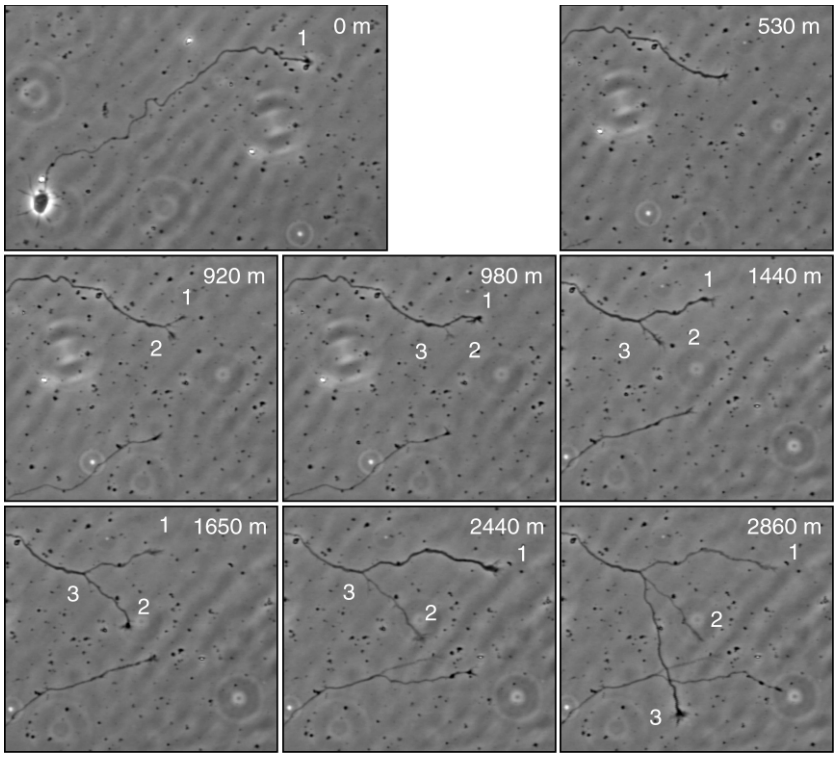

Figure 16. Elongation of axonal branches during development of cerebral cortex neurons in tissue culture. The different branches show alternating outgrowth.

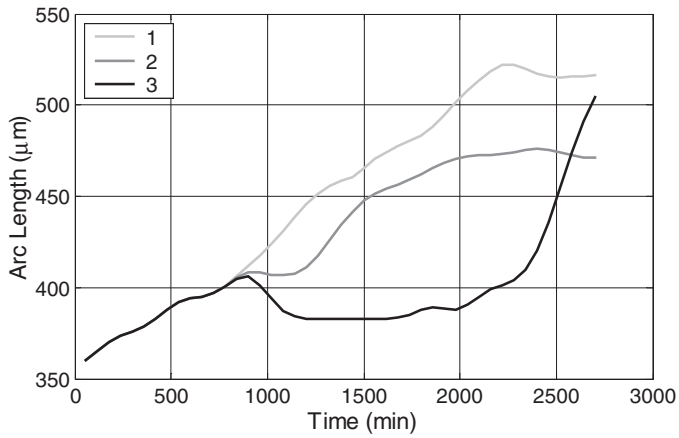

Figure 17. Arc length evolution of branches.

implementation, the proposed methodology provides a general and versatile set of concepts and tools that can be used to address a large number of problems in neuromorphometry. Special attention has been given to defining a proper formal characterization of several related issues, which has been done by using the concepts of feature space, shape trajectories, and potential spaces, as well as the respective statistical versions.

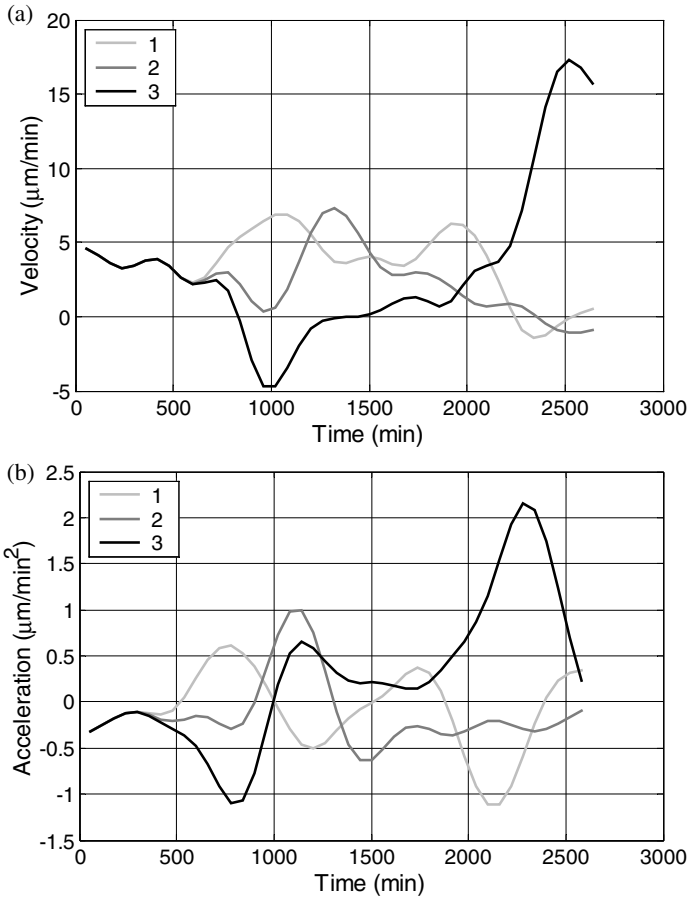

Figure 18. (a) Velocity and (b) acceleration of the axon segments.

Four families of neuromorphometric tools have been described, discussed, and illustrated with respect to the analysis of shapes of cultured neurons and of the dynamics of neuronal outgrowth:

(i) the multiscale skeletonization approach made it possible to obtain dendrogram representations from cultured neurons in an automated way;
(ii) the multiscale fractal dimension approach made it possible to characterize the shape complexity of different sets of cultured neurons;
(iii) we found a higher dispersion of complexity in the OPHN1 transfected neurons, and a lower dispersion of complexity in the RhoGAP transfected neurons in comparison with control transfected neurons; and
(iv) the spectral approach to differential geometry made it possible to determine arc lengths along a parametric curve.

With this approach the time course of elongation and acceleration rates of outgrowing axons could be quantified, clearly demonstrating strong correlations in the outgrowth rates of individual segments.

The continuation of the present work should include specific problems in 3D and dynamical shapes, as well as the use of artificial intelligence tools in order to obtain automated

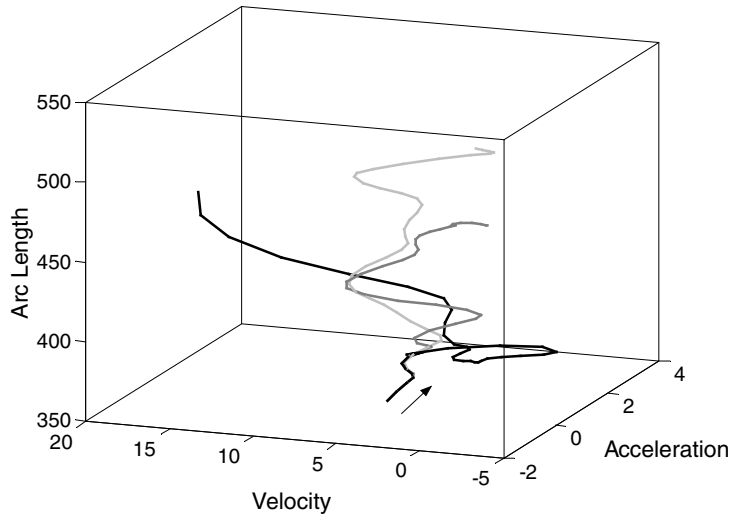

Figure 19. The shape trajectories defined by the three measures considered.

extraction of knowledge from neural data. By providing an accurate and objective quantitative characterization of the neuronal geometry, such concepts and techniques provide a valuable means for classification of nerve cells and systematic investigations about the relationship between neuronal shape and function. The extension to 3D will be particularly useful as a means of treating data obtained from 3D reconstructions, such as by using confocal microscopes which, though in a relatively incipient stage of development, are currently undergoing major advancements. Among the benefits to be expected from 3D extensions [70] we have the possibility to characterize additional angles and curvatures, as well as a series of differential measures, in such a way as to obtain a richer description and classification of the neural structures.

Acknowledgments

LdaFC is grateful to FAPESP (Procs 96/05497-3 and 99/12765-2) and CNPq (Proc 301422/92-3) for financial support. GR acknowledges the financial support of the Netherlands Epilepsy Foundation (grant NEF 20-06).

References

[1] Cajal S R 1991 *Recollections of My Life* (Cambridge, MA: MIT Press)
[2] Katz L C and Shatz C J 1996 Synaptic activity and the construction of cortical circuits *Science* **274** 1133–8
[3] Fukuda Y, Hsiao C F, Watanabe M and Ito H 1984 Morphological correlates of physiologically identified Y-, X-, and W-cells in cat retina *J. Neurophysiol.* **52** 999–1013
[4] Segev I 1998 Sound grounds for computing dendrites *Nature* **393** 207–8
[5] Koch C, Poggio T and Torre V 1982 Retinal ganglion cells: a functional interpretation of dendritic morphology *Phil. Trans. R. Soc.* B **298** 227–64
[6] Wässle H 1986 Sampling the visual space by retinal ganglion cells *Visual Neuroscience* ed J D Pettigrew and K J Sanderson (Cambridge: Cambridge University Press)
[7] Stirling R V and Dunlop S A 1995 The dance of the growth cones—where to next? *Trends Neurosci.* **18** 111–5
[8] Perry V H and Linden R 1982 Evidence for dendritic competition in the developing retina *Nature* **297** 683–5
[9] Coelho R C and Costa L F 1997 Morphologically realistic neural networks *IEEE Int. Conf. on Engineering of Complex Systems* (New York: IEEE) pp 223–8
[10] Kolb H, Nelson R and Mariani A 1981 Amacrine cells, bipolar cells and ganglion cells of the cat retina: a Golgi study *Vis. Res.* **21** 1081–114

[11] Leventhal A G and Schall J D 1983 Structural basis of orientation sensitivity of cat retinal ganglion cells *J. Comput. Neurol.* **220** 465–75
[12] Morigiwa K, Tauchi M and Fukuda Y 1989 Fractal analysis of ganglion cell dendritic branching patterns of the rat and cat retinae *Neurosci. Res.* Suppl 10, S131–9
[13] Sholl D A 1953 Dendritic organization in the neurons of the visual and motor cortices of the cat *J. Anat.* **87** 387–406
[14] Wässle H, Boycott B B and Illing R B 1981 Morphology and mosaic of on- and off-beta cells in the cat retina and some functional considerations *Phil. Trans. R. Soc.* B **212** 177–95
[15] Fuxe K and Agnati L F 1991 Two principal modes of electrochemical communication in the brain: volume versus wiring transmission *Volume Transmission in the Brain: Novel Mechanisms for Neural Transmission* ed K Fuxe and L F Agnati (New York: Raven)
[16] Nicholson C and Sykova E 1998 Extracellular space structure revealed by diffusion analysis *Trends Neurosci.* **21** 207–15
[17] Mainen Z and Sejnowski T 1996 Influence of dendritic structure on firing patterns in model neocortical neurons *Nature* **382** 363–6
[18] Duijnhouer J, Remme M W H, Ooyen A V and van Pelt J 2001 Influence of dendritic topology on firing patterns in model neurons *Neurocomputing* **38–40** 183–9
[19] Schutter E D and Steuber V 2001 Modeling simple and complex active neurons *Computational Neuroscience, Realistic Modelling for Experimentalists* ed E D Schutter (Boca Raton, FL: Chemical Rubber Company Press) pp 233–58
[20] Costa L F and Cesar R M 2001 *Shape Analysis and Classification* (Boca Raton, FL: Chemical Rubber Company Press)
[21] Soize C 1994 *The Fokker–Planck Equation for Stochastic Dynamical Systems and its Explicit Steady State Solutions* (Singapore: World Scientific)
[22] Duda R O and Hart P E 1973 *Pattern Classification and Scene Analysis* (New York: Wiley)
[23] Hilborn R C 2000 *Chaos and Nonlinear Dynamics: an Introduction for Scientists and Engineers* (New York: Oxford University Press)
[24] Ascoli G A, Krichmar J L, Nasuto S J and Senft S L 2001 Generation, description and storage of dendritic morphology data *Phil. Trans. R. Soc.* B **356** 1131–45
[25] Ascoli G A 1999 Progress and perspectives in computational neuroanatomy *Anat. Rec.* **257** 195–207
[26] Masseroli M, Bollea A and Forloni G 1993 Quantitative morphology and shape classification of neurons by computerized image-analysis *Comput. Methods Programs Biomed.* **41** 89–99
[27] DeFelipe J and Farinas I 1992 The pyramidal neuron of the cerebral-cortex—morphological and chemical characteristics of the synaptic inputs *Prog. Neurobiol.* **39** 563–607
[28] Kriegstein A R and Dichter M A 1983 Morphological classification of rat cortical-neurons in cell culture *J. Neurosci.* **3** 1634–47
[29] Caserta F, Stanley H E, Eldred W D, Daccord G, Hausman R E and Nittman J 1990 Physical mechanisms underlying neurite outgrowth: a quantitative analysis of neuronal shape *Phys. Rev. Lett.* **64** 95–8
[30] Cesar R M and Costa L F 1997 Application and assessment of multiscale bending energy for morphometric characterization of neural cells *Rev. Sci. Instrum.* **68** 2177–86
[31] Costa L F 1995 Computer vision based morphometric characterization of neural cells *Rev. Sci. Instrum.* **66** 3770–3
[32] Ramon-Moline E 1962 An attempt at classifying nerve cells on the basis of their dendritic patterns *J. Comput. Neurol.* **119** 211–27
[33] Uylings H B M, Ruiz-Marcos A and van Pelt J 1986 The metric analysis of three-dimensional dendritic tree patterns: a methodological review *J. Neurosci. Methods* **18** 127–51
[34] Van Pelt J, Uylings H B M and Verwer R W H 1989 Distributional properties of measures of tree topology *Acta Stereol.* **8** 465–70
[35] Costa L F and Velte T J 1999 Automatic characterization and classification of ganglion cells from the salamander retina *J. Comput. Neurol.* **404** 33–51
[36] Burton B P 2001 *Automated 3D Reconstruction of Neuronal Structures From Serial Sections* webpage citeseer.nj.nec.com/burton99automated.html (accessed 13 December 2001)
[37] Herzog A, Krell G, Michaelis B, Wang J, Zuschratter W and Braun K 1997 Restoration of three-dimensional quasi-binary images from confocal microscopy and its application to dendritic trees *Proc. SPIE* **2984** 146–57
[38] Boissonnat J D and Geiger B 1992 Three dimensional reconstruction of complex shapes based on the Delauney triangulation *Technical Report* 1697 (INRIA Rapports de Recherche—Sophia Antipolis)
[39] Lorensen W E and Cline H E 1987 Marching cubes: a high resolution 3d surface construction algorithm *ACM SIGGRAPH* **21** 163–9

[40] Streekstra G J, Van Den Boomgaard R and Smeulders A W M 2001 *Int. J. Comput. Vision* **42** 177–89
[41] Carmo M P 1976 *Differential Geometry of Curves and Surfaces* (Englewood Cliffs, NJ: Prentice-Hall)
[42] Bruce J W and Giblin P J 1992 *Curves and Singularities: A Geometrical Introduction to Singularity Theory* (Cambridge: Cambridge University Press)
[43] Dudek G 1997 *Shape Representation and Recognition from Multiscale Curvature* webpage www.cs.yorku.ca/∼tsotsos/complete-papers.html (Accessed 13 December 2001)
[44] Mokhatarian F and Mackworth A 1992 A theory of multiscale, curvature-based shape representation for planar curves *IEEE Trans. Pattern Anal. Mach. Intell.* **14** 789–805
[45] Cesar R M and Costa L F 1995 Piecewise linear segmentation of digital contours in O(N.LOG(N)) through a technique based on effective digital curvature estimation *Real Time Imag.* **6** 409–17
[46] Cesar R M and Costa L F 1996 Towards effective planar shape representation with multiscale digital curvature analysis based on signal processing techniques *Pattern Recognit.* **29** 1559–69
[47] Worring M and Smeulders A W M 1995 Digitized circular arcs—characterization and parameter-estimation *IEEE Trans. Pattern Anal. Mach. Intell.* **17** 587–98
[48] Worring M and Smeulders A W M 1993 Digital curvature estimation *CVGIP, Image Understand.* **58** 366–82
[49] Rui Y, She A C and Huang T S 1996 Modified Fourier descriptors for shape representation—a practical approach *Proc. 1st Int. Workshop on Image Databases and Multi Media Search* (Amsterdam)
[50] Kauppinen H, Seppanen T and Pietikainen M 1995 An experimental comparison of autoregressive and Fourier-based descriptors in 2D shape classification *IEEE Trans. Pattern Anal. Mach. Intell.* **17** 201–7
[51] Loncaric S and Dhawan A P 1993 A morphological signature transform for shape-description *Pattern Recognit.* **26** 1029–37
[52] Brandt J W 1991 Theory and application of the skeleton representation of continuous shapes *PhD Thesis* University of California, Davis, CA 5
[53] Van Pelt J and Uylings H B M 1999 Natural variability in the geometry of dendritic branching patterns *Modeling in the Neurosciences—from Ionic Channels to Neural Networks* ed R R Poznanski (Amsterdam: Harwood) pp 79–108
[54] Leyton M 1992 *Symmetry, Causality, Mind* (Cambridge, MA: MIT Press)
[55] Costa L F 1999 Particle systems analysis by using skeletonization and exact dilations *Part. Part. Syst. Charact.* **16** 273–7
[56] Costa L F and Manoel E T M 2001 Optimized approach to multiscale skeleton generation *Opt. Eng.* **40** 1752–3
[57] Costa L F and Estrozi L F 1999 Multiresolution shape representation without border shifting *Electron Lett.* **35** 1828–30
[58] Falcão A X, Costa L F and Cunha B S 2002 Multiscale skeletons image foresting transform and its application to neuromorphometry *Pattern Recognit.* at press
[59] Young I, Walker J and Bowie J 1974 An analysis technique for biological shape *Comput. Graph. Image Process.* **25** 357–70
[60] Costa L F, Campos A G and Manoel E T M 2001 An integrated approach to shape analysis: results and perspectives *Int. Conf. on Quality Control by Artificial Vision* pp 23–34
[61] Montague P R and Friedlander M J 1991 Morphogenesis and territorial coverage by isolated mammalian retinal ganglion cells *J. Neurosci.* **11** 1440–57
[62] Kauffman W E and Moser H W 2000 Dendritic anomalies in disorders associated with mental retardation *Cereb. Cortex* **10** 981–91
[63] Chelly J and Mandel J L 2001 Monogenic causes of X-linked mental retardation *Nat. Rev. Genet.* **2** 669–80
[64] Luo L 2000 Rho GTPases in neuronal morphogenesis *Nat. Rev. Neurosci.* **1** 173–80
[65] Ramakers G J A 2002 Rho proteins, mental retardation and the cellular basis of cognition *Trends Neurosci.* **25** 191–9
[66] Billuart P *et al* 1998 Oligophrenin-1 encodes a RhoGAP protein involved in X-linked mental retardation *Nature* **392** 923–6
[67] Ramakers G J A, Winter J, Hoogland T M, Lequin M B, Van Hulten P, van Pelt J and Pool C W 1998 Depolarization stimulates lamellipodia formation and axonal but not dendritic branching in cultured rat cerebral cortex neurons *Dev. Brain Res.* **108** 205–16
[68] Ridley A J, Self A J, Kasmi F, Paterson H F, Hall A, Marshall C J and Ellis C 1993 Rho family GTPase activating proteins p190, bcr and RhoGAP show distinct specificities *in vitro* and *in vivo* *EMBO J.* **12** 5151–60
[69] Nakayama A Y, Harms M B and Luo L 2000 Small GTPases Rac and Rho in the maintenance of dendritic spines and branches in hippocampal pyramidal neurons *J. Neurosci.* **20** 5329–38
[70] Worring M, Pfluger P, Smeulders A W M and Houtsmuller A B 1994 Measurement of 3D-line shaped objects *Pattern Recognit. Lett.* **15** 497–506